

An Active Coupling Mechanism with Three Modes of Operation for Modular Mobile Robotics

Paul M. Moubarak, *Student Member, IEEE*, Pinhas Ben-Tzvi, *Senior Member, IEEE*
Zhou Ma, *Student Member, IEEE*, Eric J. Alvarez

Abstract—This paper presents a new design for a docking interface that enables rigid, reversible and non-back-drivable coupling between robotic modules in a chain architecture. The distinctive merit of the proposed interface is exhibited in its ability to operate in three independent modes. In the *drive mode*, the motor torque is directed to drive the host module. In the *neutral mode*, the motor torque aligns the coupling elements prior to docking. In the *clamp mode*, the motor torque actuates the revolute joint resulting from this docking process, thus allowing one module to revolve relative to its neighbors in the formation. In this paper, an optimality analysis of the unique kinematic properties of the dual-rod slider-rocker (DRSR) mechanism which enables this tri-state operation is presented. This analysis is supplemented by simulations and experimental results that validate these optimal kinematics, as well as the rigidity and the three operation modes of the docking interface.

I. INTRODUCTION

DOCKING in modular mobile robotics refers to the process by which two or more independent mobile agents bind together to create a larger and more capable formation. This scalability in size and shape allows the resulting chain or lattice architecture [1] to exhibit mobility patterns [2], [3] or execute manipulation tasks that would otherwise be impossible to achieve with a single module.

At the core of this reconfiguration lies a coupling interface that connects modules together in a desired formation. However, for field mobility and manipulation applications, such interfaces are required to meet the following three main structural constraints, among others:

- Rigidity*: to enable the scaled architecture to exhibit strength attributes comparable to a rigid-structure robot.
- Reversibility*: to enable the scaled formation to undock and revert back to individual mobility.
- Non-back-drivability*: to prevent the undesirable detachment of modules in a formation under excessive loading.

In the literature, a multitude of different techniques have thus far been explored for the development of bonding mechanisms in modular robotics, including mechanical

grippers, magnets [2], [3], mechanical connectors [4],[5] vacuum [6] and latching mechanisms actuated by Shape Memory Alloys (SMA) [7], [8] (a more comprehensive tabular comparison of bonding mechanisms in modular robotics can be found in [9]). However, despite the different shape formations demonstrated in reconfigurable robotics [2] – [10],[13] the ability of a modular mobile robot to deliver high-capacity manipulation is yet to be proven. In fact, with existing technology of active docking, a fixed-structure mobile robot tailored to perform a specific task is more likely to outperform its modular counterpart, due to the lack of rigidity in traditional coupling [11]. This subsequently limits the payload capacity and the usability of the overall formation in field operations.

In this paper, we address this problem by proposing a new design for active docking that provides rigid, reversible and non-back-drivable mechanical coupling between modular mobile robots in a chain architecture. The motivations of this work stem from STORM – Self-configurable and Transformable Omni-directional Robotic Modules (Fig. 1), which represents an on-going research investigation for modular mobility and manipulation on unstructured terrain. The overall articulated structure of STORM was inspired by the design of the Hybrid Mechanism Mobile Robot [14-16].

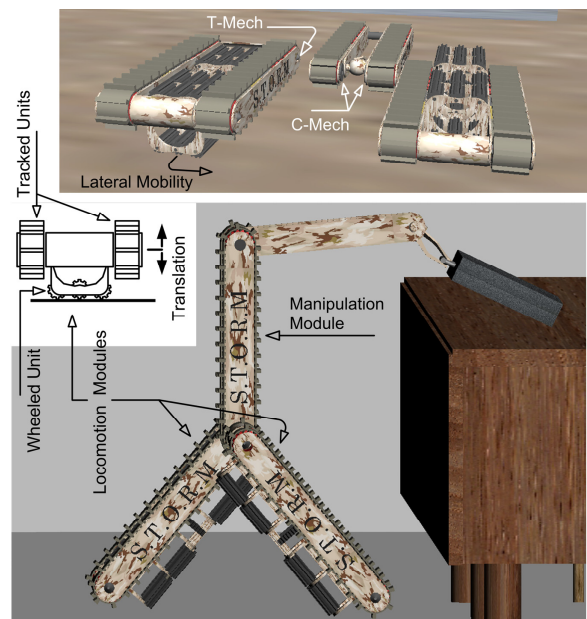


Fig. 1. An illustration of STORM showing the locomotion and manipulation modules, the two elements of the docking interface (*C-Mech* and *T-Mech*) and a three module humanoid formation

Manuscript received September 17, 2012. This work is supported by the Robotics and Mechatronics Lab in the School of Engineering & Applied Sciences at the George Washington University, Washington, DC 20052, USA

P. M. Moubarak, Z. Ma are Doctoral students; E. J. Alvarez is an undergraduate student, all in the Department of Mechanical and Aerospace Engineering at the George Washington University, Washington DC (Phone #: 202-994-4666; e-mail: paul4@gwu.edu; mazhou@gwu.edu; eric228@gwu.edu).

P. Ben-Tzvi is an Assistant Professor of Engineering and the Director of the Robotics and Mechatronics Lab at the George Washington University, Washington, DC (Phone #: 202-994-6149; e-mail: bentzvi@gwu.edu).

STORM consists of two categories of modules: a locomotion module with a hybrid wheeled-tracked multi-directional mobility, and a manipulation module carrying a central one link arm and an end-effector (Fig. 1). The tri-state interface is split evenly between these two modules, and consists of a male element called *T-Mech* (Translational Mechanism) carried by the locomotion module, and a female element called *C-Mech* (Clamping Mechanism) typically carried by the manipulation module.

The first merit of the proposed coupling lies in the ability to operate in three independent modes. The second merit is evidenced in the use of the dual-rod slider rocker (DRSR) mechanism, which represents a new mechanism that toggles between the three modes of operation. Through the DRSR, the interface uses a single *high-torque* motor to drive the module, align the clamping elements prior to docking, and provide joint actuation to rotate one module relative to its neighbor in the formation. The details of this interface are presented in this paper, along with an optimality analysis for the synthesis of the DRSR. Simulation and experimentation results validate the unique kinematics of the DRSR, and visualize the operation modes of the interface.

II. OVERVIEW OF THE TRI-STATE DOCKING INTERFACE

The proposed tri-state docking interface is designed to meet the requirements of compactness, rigidity, reversibility, and has its male part comprised of a telescopic docking shaft that can be deployed by one module in the formation. This non-back-drivable shaft, shown in Fig. 2, is driven by a rack and pinion, and has its motion constrained to a translation by appropriate linear bearing supports. The head of the shaft further provides a hexagonal neck that mates with two semi-hexagonal apertures carried by two clamps (Fig. 2).

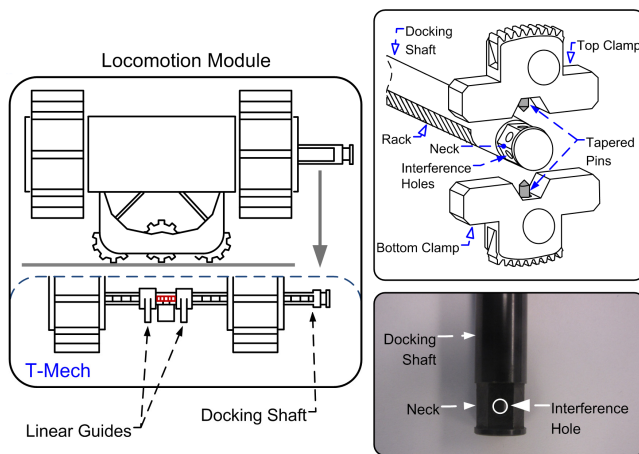


Fig. 2. Schematic of the docking mechanism and the locomotion module showing the *T-Mech*'s docking shaft and its prototype

The clamps on the other hand represent the main element of the female part, or the *C-Mech*. These clamps slide along two parallel rails, guided by linear bearings, where their translational motion is initiated by a DRSR as will be further discussed in Fig. 8. The rocker of this mechanism is driven by a selection geared-motor through a worm and worm gear

assembly (Fig. 3), which ensures the *mechanical* non-back-drivability of the interface, and enables the module carrying the *C-Mech* to dock with an adjacent module carrying the *T-Mech*. An example of such docking is provided in [12].

Each clamp of the *C-Mech* carries a pin that mates with a corresponding hole on the neck of the docking shaft. This coupling is guided by the pins' tapered tip (Fig. 2), and creates a physical interference between the mating elements which significantly increases the *structural* rigidity of the interface as will be further discussed in section V.

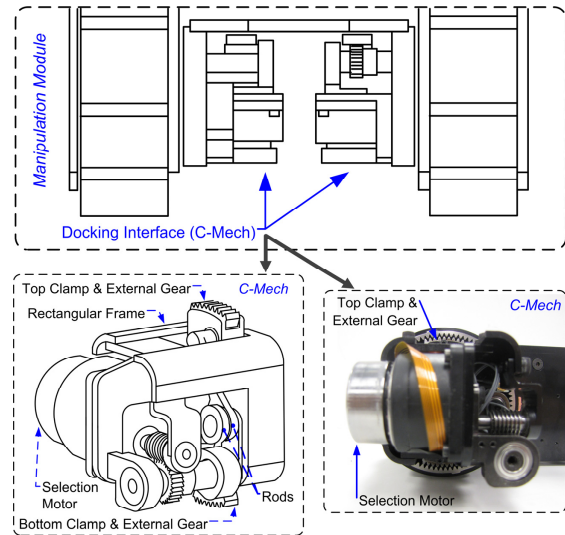


Fig. 3. Schematic of the *C-Mech* and its actual proof-of-concept prototype showing the top and bottom clamps

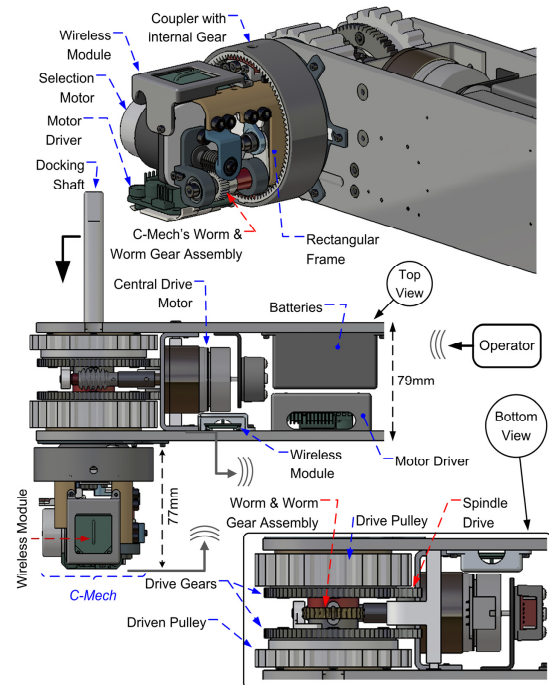


Fig. 4. CAD model of the *C-Mech* connected to a small mobile robot

Each clamp also carries an external gear segment (Fig. 2, 3) that engages the coupler's internal gear. This coupler connects rigidly to the module's pulleys (or wheels), as

shown in the transmission schematic of Fig. 5. The rectangular frame that houses the *C-Mech* is connected to a hollow main shaft supported by ball bearings, while itself providing linear bearing support for the pulleys (Fig. 5). This shaft carries a worm gear in the center, which transmits the torque (35 Nm) of a central motor to the rectangular frame and all the elements connected to it, causing the *C-Mech* to rotate at the same speed as the main shaft.

The *C-Mech*'s electrical components are powered by a Li-Ion battery (22V) carried by the module. Electricity is transmitted from the module to the *C-Mech* via two pairs of graphite brushes (Fig. 4) that create a contact with two PCB's (PCB-F and PCB-C), thus enabling the *C-Mech* to rotate endlessly inside the coupler. Sensor and motor command data is transmitted between the *C-Mech*, the module and the operator through a local wireless network created with X-Bee RF transceivers (2.4 GHz) (Fig. 4).

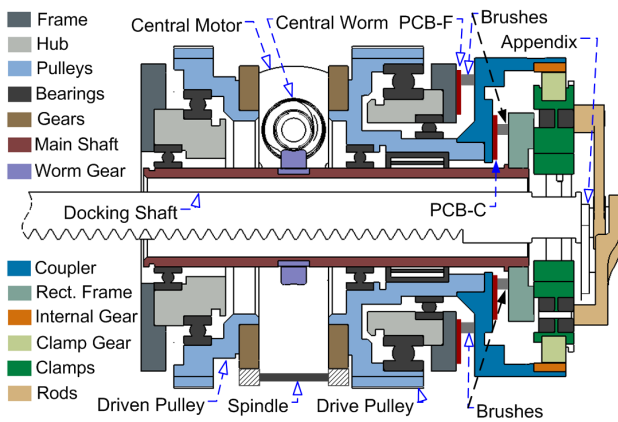


Fig. 5. Simplified transmission schematic of the *C-Mech*, the pulleys and the central motor assembly

III. MODES OF OPERATION

The proposed docking interface operates in three modes: *Drive*, *Neutral* and *Clamp*, which can be visualized in the video file in [12]. These modes are initiated via an appropriate positioning of the clamps along the rails enabled by the DRSR mechanism. The DRSR was selected due to its significantly smaller footprint as compared to other non-back-drivable 1-DOF mechanisms such as a lead screw.

A. Drive Mode

In this mode, the selection motor rotates in a direction to slide the clamps outwards until the clamp gear segments

engage the internal gear of the coupler as shown in Figs. 6(a), 7(a). This engagement is monitored by a linear encoder (5V TTL, Mercury 1520P-L30 series) which measures the total displacements of the clamps along the rails. Once this engagement is initiated, the torque generated by the central motor will be transmitted to the coupler, causing the drive pulley/wheel to rotate at the same speed as the coupler.

B. Neutral Mode

In the *neutral mode*, the clamps are positioned somewhere in the middle stroke of the sliders in a way to disengage the clamp gear segments from the internal gear as shown in Figs. 6(b), 7(b). When this disengagement occurs, the actuation of the central motor causes the *C-Mech* to rotate freely inside the coupler, enabling the alignment of the protruding pins with the interference holes prior to coupling.



Fig. 6. Proof of concept prototype of the docking interface, showing the positions of the sliders corresponding to the three modes of operation

C. Clamp Mode

In this mode, the selection motor is rotated in a direction to slide the clamps downwards along the rails until the pins and the combined semi-hexagonal pockets of the clamps mate with the holes and the hexagonal neck of the docking shaft, respectively (Figs. 6(c), 7(c)). This interference locks the shaft and the sliders together, and prevents one from sliding away or rotating relative to the other.



Fig. 7. The three modes of operation of the proposed coupling mechanism, a) *Drive*, b) *Neutral*, c) *Clamp*

When this happens, the central worm gear behaves as a sun, and the worm as a planet. This converts the rotation of the central motor to a planetary revolution of the whole module around the docking shaft which creates the joint axis for this rotation. In such case, the mobility of the formation will be provided by the adjacent modules, since the motor torque of the module carrying the *C-Mech* will be re-directed to rotate it around its neighbors in this mode [12].

IV. OPTIMAL DESIGN OF THE DRSR MECHANISM

A. Kinematic Analysis

In order to derive the kinematics of the proposed DRSR mechanism, we first define an appropriate nomenclature in reference to Fig. 8.

$X_0Y_0Z_0$	Global Cartesian frame
l_1, l_2, l_2'	Length of the rocker, the top rod and the bottom rod, respectively
$\theta_1, \theta_2, \theta_2'$	Rocker angle, top rod angle and bottom rod angle relative to the Y_0 -axis, respectively
b, b'	Distance between Y_0 -axis and the top and bottom rod/slider joint axis along X_0 -axis, respectively
h	Distance between the top rod/slider joint axis and the bottom edge of the top slider, along Y_0 -axis
h'	Distance between the bottom rod/slider joint axis and the top edge of the bottom slider, along Y_0 -axis
c	Distance between X_0 -axis and the central plane, measured along Y_0 -axis
y, y'	Distance between bottom (top) edge of top (bottom) slider and the central plane, measured along Y_0 -axis
y_{\max}	Stroke length of each slider, also defined as the position of the <i>drive</i> terminal boundary condition
$\theta_{1,y_0}, \theta_{1,y_{\max}}$	Rocker angle at $y = 0$ and $y = y_{\max}$, respectively

Because of the kinematic dependency that exists between θ_1 and (θ_2, θ_2') due to the restriction of the sliders' motion to a translation along the Y_0 -axis, it becomes possible to express the dual-rod angles in terms of the rocker angle θ_1 as

$$\sin(\theta_2) = \frac{l_1 \sin(\theta_1) + b}{l_2} \quad (1)$$

$$\sin(\theta_2') = \sin(\pi - \theta_2') = \frac{l_1 \sin(\theta_1) + b'}{l_2'} \quad (2)$$

Equations (1) and (2) can be further employed to derive expressions for y and y' , which can be written as

$$y = l_1 \cos(\theta_1) + l_2 \sqrt{1 - \left\{ \frac{l_1 \sin(\theta_1) + b}{l_2} \right\}^2} - c - h \quad (3)$$

$$y' = l_1 \cos(\theta_1) - l_2' \sqrt{1 - \left\{ \frac{l_1 \sin(\theta_1) + b'}{l_2'} \right\}^2} - c + h' \quad (4)$$

where based on axes X_0Y_0 defined in Fig. 7, $y > 0$ & $y' < 0$.

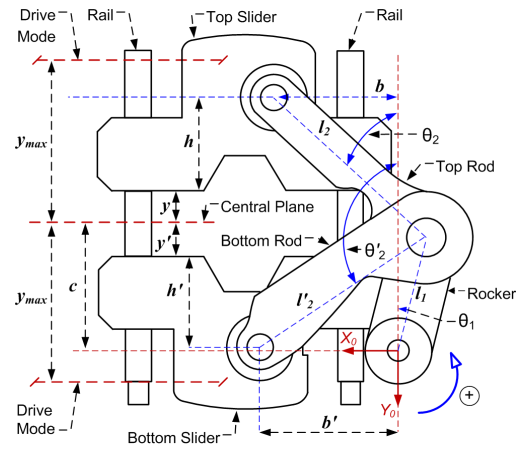


Fig. 8. Kinematics of the dual-rod slider rocker (DRSR) mechanism

In (3) and (4), y and y' are an explicit function of θ_1 . This means that the displacement offset between the top and bottom sliders, defined by $e = y + y'$, varies in terms of θ_1 . This implies that the two sliders do not travel the same distance for the same rocker rotation, which means that the clamps are neither able to reach the central plane, nor engage the internal gear at the same time.

B. Optimality analysis

In order to meet the boundary conditions that define the *C-Mech's* *drive* and *clamp* modes, the DRSR should be designed to minimize the offset e defined as

$$e = f(\theta_1, b, l_1, l_2, b', l_2', h, h', c, \theta_{1,y_0}, \theta_{1,y_{\max}}, y_{\max}) \quad (5)$$

The expression in (5) can be reduced if one accounts for the geometric constraints imposed by the sliders' design, as well as the kinematic dependencies that exist between the different parameters of (5).

If the top slider/rod are selected as a reference for this analysis, the first objective will be to maximize the push/pull (Y_0 -axis) component of the force transmitted to the top slider through the top rod. This can be achieved by selecting the minimum allowable value of b and the maximum allowable value of h that the dimensions of the slider tolerate. Similarly, a combination of l_1, c and θ_{1,y_0} can be selected to satisfy other geometric constraints, such as preventing interference between the rocker and the ground at the *clamp* mode by containing the rocker inside the coupler's circumference (*i.e.* Fig. 6(c)). These selected values enable the calculation of l_2 as

$$l_2^2 = l_1^2 + b^2 + (c + h)^2 - 2l_1 \sqrt{b^2 + (c + h)^2} \cos\left(\theta_{1,y_0} + \text{tg}^{-1}\left\{\frac{b}{c + h}\right\}\right) \quad (6)$$

and the computation of $\theta_{1,y_{\max}}$ as

$$\theta_{1,y_{\max}}^{1,2} = \sin^{-1}\left(\frac{-\rho b \pm p \sqrt{p^2 - \rho^2 + b^2}}{b^2 + p^2}\right) \quad (7)$$

where $p = c + h + y_{\max}$. Equation (7) is satisfied for an *elbow-up* and an *elbow-down* posture of the rocker and rods, where only the *elbow-up* solution ($\theta_{1,y_{\max}}^1$) is possible due to gear engagement at the *drive mode*.

This choice of parameters reduces e in (5) to $e = f(\theta_1, b', l_2', h')$. However, because such offset is a direct function of θ_1 , there exist no unique values for b' , h' and l_2' that generate a zero-offset profile over the entire range $\theta_{1,y_{\max}} \leq \theta_1 \leq \theta_{1,y_0}$. Nonetheless, b' , h' and l_2' can be calculated to satisfy the *drive* $y' = y_{\max}|_{\theta_{1,y_{\max}}}$, and *clamp* $y' = 0|_{\theta_{1,y_0}}$ boundary conditions, while truncating the offset in the intermediate stroke to an acceptable threshold.

An expression for l_2' is derived by considering the geometry of the mechanism at the *clamp* boundary condition which ensures the non-violation of this constraint $\forall b', h'$. This equation is expressed in terms of b' and h' as

$$l_2'^2 = l_1^2 + q^2 - 2ql_1 \cos(\beta + \theta_{1,y_0}) \quad (8)$$

where

$$q = \sqrt{b'^2 + (c - h')^2}, \quad \beta = \text{tg}^{-1} \left\{ \frac{b'}{c - h'} \right\}$$

The substitution of (6) into (3), and (8) into (4) generates an offset e in terms of θ_1 , b' and h' , as follows

$$e(\theta_1, b', h') = 2l_1 \cos \theta_1 + \sqrt{l_2'^2 - (l_1 \sin \theta_1 + b')^2} - 2c - h + h' - \sqrt{b'^2 + (c - h')^2 + l_1^2 - \left(2\sqrt{b'^2 + (c - h')^2} \right) - \left[l_1 \cos \left\{ \theta_{1,y_0} + \text{tg}^{-1} \left(\frac{b'}{c - h'} \right) \right\} - (l_1 \sin \theta_1 + b')^2 \right]} \quad (9)$$

Because the *clamp* boundary condition is guaranteed through (8), equation (9) can be minimized at $\theta_{1,y_{\max}}$ to generate an optimal combination of b' and h' that can meet the *drive* boundary condition $y' = y_{\max}|_{\theta_{1,y_{\max}}}$.

However, this cost function should be further supplemented by the efficiency of the bottom slider-rocker as a second objective function defined as

$$\zeta(\theta_1, b', h') = \sqrt{1 - \left(\frac{l_1 \sin(\theta_1) + b'}{l_2'} \right)^2} \quad (10)$$

which delineates the ratio $\zeta(\%) = \left({}^0F_{Brod} \right)_{Y_0} / {}^0F_{Brod}$, where ${}^0F_{Brod}$ defines the force transmitted by the bottom rod and expressed in the global frame, and $\left({}^0F_{Brod} \right)_{Y_0}$ the component of ${}^0F_{Brod}$ along the Y_0 -axis. Furthermore, because e is left

unbounded in the *neutral mode*, it becomes necessary to cap the supremum of $e(\theta_1, b', h')$ to an acceptable threshold δ .

All these considerations are aggregated into a multi-objective optimization problem whose solution generates an optimal pair $(b', h')^{opt}$ which enables the mechanism to meet the terminal boundary conditions. This problem is stated as

$$\begin{aligned} & \text{Min} && e(\theta_1, b', h')|_{\theta_{1,y_{\max}}} \\ & b', h' \in \Omega && \\ & \text{Max} && \zeta(\theta_1, b', h')|_{\theta_{1,y_{\max}}} \\ & b', h' \in \Omega && \end{aligned} \quad (11)$$

subject to $\sup |e(\theta_1, b', h')| < \delta$

and the set of geometric constraints $\Omega = \begin{cases} b'_{\min} \leq b' \leq b'_{\max} \\ h'_{\min} \leq h' \leq h'_{\max} \end{cases}$

where b'_{\min} , b'_{\max} , h'_{\min} , h'_{\max} define the limits of the allowable range of values for b' and h' , respectively.

C. Case-Study Solution and Simulation

A case-study solution for the design problem stated in (11) is visualized in Fig. 9, for $18.5 \leq b' \leq 26.5$ and $10.5 \leq h' \leq 14.4$, with $l_1 = 17.7 \text{ mm}$, $c = 19 \text{ mm}$, $b = 18.1 \text{ mm}$, $\theta_{1,y_0} = 27^\circ$, $\theta_{1,y_{\max}} = -4.05^\circ$, $y_{\max} = 11 \text{ mm}$, $h = 14.1 \text{ mm}$ and $\delta = 0.6 \text{ mm}$. This solution is decomposed into five subsets, where only the optimal subset contains the pairs (b', h') that don't violate any constraints. Since ζ increases with b' and h' , one would chose an optimal pair $(b', h')^{opt}$ that belongs to the top zone of the optimal subset. That is, for this case-study, at $b' = 21.02 \text{ mm}$, $h' = 14.39 \text{ mm}$ and $\zeta = 35.5\%$.

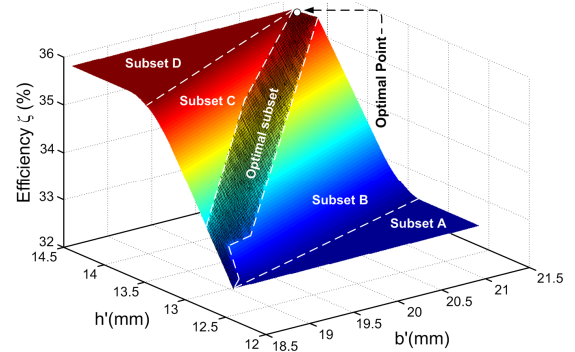


Fig. 9. Meshed space solution of the optimization problem in (11)

The feasibility of this optimal solution is validated through a kinematic simulation of the DRSR mechanism. The results of this simulation are shown in Fig. 10 for a case-study rocker velocity of $\dot{\theta}_1 = 20^\circ/s$, whereby the scenario in which the mechanism is driven down from the *drive mode* toward the *clamp mode* is considered. This simulation proves that the optimal dimensions of the DRSR enable the two sliders to travel away from the *drive mode* and reach the *clamp mode* simultaneously, in spite of the relative displacement offset that exists in the intermediate stroke.

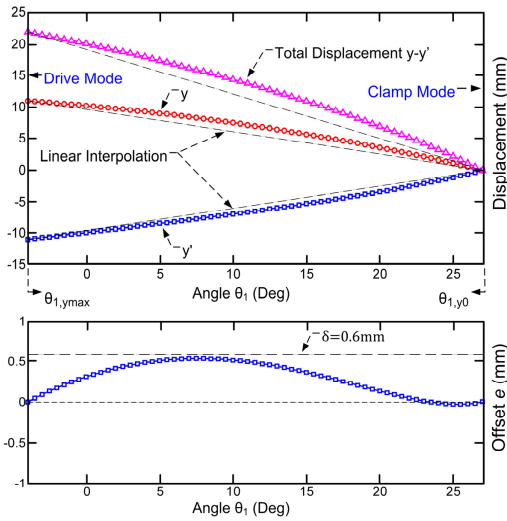


Fig. 10. Displacements of the top clamp (y), bottom clamp (y'), total distance separating both clamps ($y-y'$), and relative translation offset plotted as a function of θ_1

V. DOCKING RIGIDITY

The tapered pins added to the two clamps play a major role in strengthening the rigidity of the interface. Through their interference with the holes of the docking shaft, the pins eliminate the force component along the rails which tends to separate the clamps under joint loading in the *clamp mode*. Instead, the two clamps are twisted together as a rigid body, which prevents separation and redirects the load from the rocker and the selection motor driving it, to the rails.

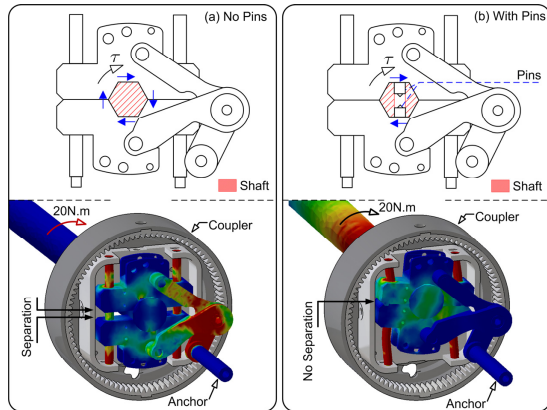


Fig. 11. Finite Element Analysis showing the role the pins play in preventing clamp separation in the *clamp mode* (a) no pins (b) with Pins

This behavior is reflected in the finite element analysis in Fig. 11, which compares a case of no interference to a case of interference created by the pins. Because the load is redirected toward the rails, the strength of this interface become independent of the *C-Mech's* worm and worm gear assembly, and rather turns it into a design parameter that can be amplified via an appropriate dimensioning of the rails and pins. This increases the torque capacity of the interface, where we further measured a 45 Nm torque loading with the prototype about the weakest axis (torsion axis) prior to pin yielding. This measurement is 90% higher than the highest torque capacity of an active docking interface reported in the literature (23.5N.m, JL-2 [10]).

VI. CONCLUSION AND FUTURE WORK

This paper presented the design, analysis and implementation of a new tri-state rigid, reversible, and non-back-drivable docking interface for modular robotics. The interface uses a dual-rod slider rocker (DRSR) mechanism to toggle between its three operation modes. The DRSR further strengthens the torque capacity by creating a physical interference with the docking shaft. In the future, we continue our investigations by exploring the interface's integration on a three-module formation of STORM.

REFERENCES

- [1] M. Yim, W.-M. Shen, B. Salemi, D. Rus, M. Moll, H. Lipson, E. Klavins, and G. S. Chirikjian, "Modular Self-reconfigurable Robot Systems: Challenges and Opportunities for the Future," *IEEE Robotics and Automation Magazine*, vol.14, no. 1, pp. 2 – 11, Mar. 2007.
- [2] H. Wei, Y. Chen, J. Tan, and T. Wang, "Sambot: A Self-Assembly Modular Robot System," *IEEE/ASME Trans. Mechatronics*, vol. 16, no. 4, pp. 745 – 757, Aug. 2011.
- [3] H. Kurokawa, A. Kamimura, E. Yoshida, K. Tomita, S. Kokaji, and S. Murata, "M-TRAN II: Metamorphosis from a Four-legged Walker to a Caterpillar," in *Proc. IEEE/RSJ Int. Conf. Intelligent Robots and Systems (IROS '03)*, Nevada, 2003, pp. 2454 – 2459.
- [4] W.-M. Shen, M. Krivokon, H. Chiu, J. Everist, M. Rubenstein, and J. Venkatesh, "Multimode Locomotion via SuperBot Reconfigurable Robots," *J. Autonomous Robots*, vol. 20, no. 2, pp. 165 – 177, 2006.
- [5] M.W. Jorgenson, E.H. Østergaard, and H.H. Lund, "Modular ATRON: Modules for a Self-reconfigurable Robot" In *Proc. IEEE/RSJ International Conference on Intelligent Robots and Systems (IROS '04)*, Japan, 2004, pp. 2068 – 2073.
- [6] R.F.M. Garcia, J.D. Hiller, K. Stoy, and H. Lipson, "A Vacuum-Based Bonding Mechanism for Modular Robotics," *IEEE Trans. on Robotics*, vol. 27, no. 5, pp. 876 – 890, Oct. 2011.
- [7] M. Yim, D. Duff, and K. Roufas, "PolyBot: a Modular Reconfigurable Robot," in *Proc. IEEE International Conference on Robotics and Automation (ICRA'00)*, California, 2000, pp. 514 – 520
- [8] H.B. Brown, J.M. Vande Weghe, C.A. Bererton, and P.K. Khosla, "Millibot Train for Enhanced Mobility," *IEEE/ASME Trans. on Mechatronics*, vol. 7, no. 4, pp. 452 – 461, Dec. 2002.
- [9] P. Moubarak, P. Ben-Tzvi, "Modular and Reconfigurable Mobile Robotics," *J. Robotics and Autonomous Systems*, vol. 60, no. 12, pp. 1648–1663, December 2012.
- [10] W. Wang, W. Yu, and H. Zhang, "JL-2: A Mobile Multi-Robot System with Docking and Manipulating Capabilities," *International Journal of Advanced Robotic Systems*, vol.7, no. 1 pp. 009 – 018, Fe. 2010.
- [11] M. Delrobaei, and K.A. McIsaac, "Connection Mechanism for Autonomous Self-Assembly in Mobile Robots," *IEEE Trans. Robotics*, vol. 25, no. 6, pp. 1413 – 1419, December 2009.
- [12] P. Moubarak, P. Ben-Tzvi, E. Alvarez, and Z. Ma, Demonstration of the Three Modes of Operation of the Tri-state Docking Interface, <http://www.seas.gwu.edu/~bentzvi/STORM/DOK2.html>, available: 2012.
- [13] M.D.M. Kutzer, M.S. Moses, C.Y. Brown, D.H. Scheidt, G.S. Chirikjian, M. Armand, "Design of a new independently-mobile reconfigurable modular robot," in *Proc. IEEE International Conference on Robotics and Automation (ICRA'10)*, Anchorage, Alaska, 2010, pp. 2758–2764.
- [14] P. Ben-Tzvi, "Experimental Validation and Field Performance Metrics of a Hybrid Mobile Robot Mechanism", *Journal of Field Robotics*, vol. 27, no. 3, pp. 250–267, May 2010.
- [15] P. Ben-Tzvi, A.A. Goldenberg, J.W. Zu, "Design and Analysis of a Hybrid Mobile Robot Mechanism with Compounded Locomotion and Manipulation Capability", *Journal of Mechanical Design, Transactions of the ASME*, vol. 130, no. 7, pp. 1–13, July 2008.
- [16] P. Ben-Tzvi, A.A. Goldenberg, J.W. Zu, "Design, Simulations and Optimization of a Tracked Mobile Robot Manipulator with Hybrid Locomotion and Manipulation Capabilities", *Proceedings of the 2008 IEEE International Conference on Robotics and Automation (ICRA2008)*, Pasadena, California, 2008, pp. 2307–2312.